Tunable perovskite-based photodetectors in optical sensing

Joshua Wolanyk[a,b,c], Xun Xiao[d], Michael Fralaide[a,e], Nicholas J. Lauersdorf[d], Rajiv Kaudal[a,b], Erik Dykstra[a,b], Jinsong Huang[d,**], Joseph Shinar[a,b,*], Ruth Shinar[c,e,***]

[a] *Ames Laboratory, USDOE, Iowa State University, Ames, IA 50011, United States*
[b] *Physics & Astronomy Department, Iowa State University, Ames, IA 50011, United States*
[c] *Microelectronics Research Center, Iowa State University, Ames, IA 50011, United States*
[d] *Applied Physical Sciences Department, University of North Carolina, Chapel Hill, NC 27599, United States*
[e] *Electrical & Computer Engineering Department, Iowa State University, Ames, IA 50011, United States*

ABSTRACT

Broad- and narrow-band, tunable perovskite photodetectors (PPDs) with size-dependent fast response times are demonstrated for the first time in optical sensing of analytes, including gas-phase and dissolved oxygen (DO), as well as glucose. The sensors included a LED excitation source and a polystyrene film with embedded oxygen-sensitive dyes, PtOEP or PdOEP. The analyte's dose-dependent photoluminescence (PL) intensity I and decay time τ were measured. Using the PPDs enabled monitoring gas-phase O_2 at levels of 0 %–100 % with a sensitivity comparable to that of a Si photodiode. A broad dynamic range was similarly observed for DO monitoring and the limit of detection for glucose monitoring was ~ 0.02 mM at an initial level of ~ 0.26 mM DO. Importantly, the size-dependent fast response time of the PPDs enabled analyte monitoring *via* the preferred measurement of τ, rather than I, over a broad dynamic range, which was unattainable with organic photodetectors. The use of the narrow-band PPDs eliminated the need for optical filters, which leads to more compact device designs.

1. Introduction

There is a continued and growing need for miniaturization of sensors [1,2] to enable their integration into existing and developing technologies, such as wearable electronics [3]. In the long run, such sensors will be fully adapted for applications in medical testing, security inspection, and water and food quality monitoring [4]. In parallel, organic semiconductor-based devices *e.g.*, organic light emitting diodes (OLEDs), organic solar cells (OSCs), and organic photodetectors (OPDs) continue to attract extensive interest, with OLEDs already successfully commercialized and OSCs gaining renewed interest due to recent reports of enhanced performance [5–7]. The use of the latter has broadened in *e.g.*, medical tools [8,9], photodetectors (PDs) in optical (bio) chemical sensors [10], and spectrometers-on-a-chip [11,12]. In particular, thin-film organic components can be fabricated on flexible plastic substrates, enabling development of wearable sensors and other bendable devices. Organic components are easily structurally-integrated, and hence will enable device portability and field-deployability. Hybrid perovskite-based photodetectors (PPDs) are of special interest for such

optical sensing due to their exceptional attributes of high responsivity and fast response [13,14], though their use in specific optical monitoring of analytes is yet to be demonstrated.

Thin film-based optical sensors, for (bio)chemical analyte monitoring, which are compact with a potential for miniaturization, have been demonstrated, including simultaneous detection of multiple analytes [10]. Such sensors employed, for example, OLED excitation sources and thin film PDs for signal monitoring. The PDs were based on inorganic materials such as hydrogenated amorphous Si (a-Si:H) [15] and nano-crystalline (nc) Si [16], or were OPDs [12]. The latter turned out to be more promising in comparison to a-Si:H- or nc-Si- based PDs, largely due to their faster response time and lower dark currents [17]. Long-term stability issues that some organic electronic devices face are not a major issue for such sensors, because the sensing elements are often suitable for only short-period usage, and in particular low-cost disposable sensors are often desirable. Still, encapsulated organic devices have long operational lifetimes, as demonstrated by commercial OLEDs.

While OPDs show promise as flexible devices, further improvement

in their performance is hindered by low carrier mobility and in particular relatively slow response [18]. Strategies for improving the performance of OPDs and PPDs as well as extending their spectral response are ongoing [19,20].

In contrast to OPDs, PPDs have fast response times, high carrier mobility, high external quantum efficiency (EQE), and excellent sensitivity to low light intensities. Indeed, the potential of such hybrid PDs was demonstrated in various applications. As an example, a PPD with a sub-ns response time, which is promising for imagers in digital cameras, was used for measuring the photoluminescence (PL) lifetimes of organic and hybrid materials [21,22]. Such measurements provide information on materials' quality, as the PL decay times are influenced by defects and impurities [22].

Development of hybrid PDs, including narrow-band devices, is ongoing. For example, (i) PPDs showing high gain were fabricated by trap- and interface-engineering using a perovskite rich in PbI_2 [23] and (ii) tunable, narrow band (*e.g.*, EQE with full width half maximum, FWHM $\sim$ 28 nm) PPDs were fabricated using a two-perovskite layer structure with the first, electrically inactive, thin layer filtering unwanted light, while the second being the electro-optically active layer. The sensitivity and wavelength range of such PPDs can be tuned by changing the bromine:iodine ratio in *e.g.*, $CH_3NH_3PbBr_{3-x}I_x$ in both layers; other mixtures, including chlorides, were also reported [13]. As we show, the advantage of narrow-band PPDs in sensing applications is that they do not require an external optical filter, which is otherwise needed to prevent the excitation source or stray light from reaching the PD. As such, they are more compact and easier to integrate with the other sensor components.

Other strategies based on different mechanisms for generating NB photodiodes have been reported [24–27]. These include charge collection narrowing (CCN) and charge injection narrowing (CIN). CCN is based on the concept that light with different wavelengths has different charge collection efficiency due to different penetration depths; it was demonstrated for OPDs and PPDs. CIN was only demonstrated in OPDs, resulting in photomultiplication and FWHM $\sim$ 30 nm. The narrow band in this case was attributed to the sharp absorption edge of a P3HT:PCBM (100:1 w/w) active layer with a small amount of acceptor.

In this work, we demonstrate for the first time the suitability of PPDs for optical analyte sensing by monitoring not only dose-dependent changes in the PL intensity I of analyte-sensitive dyes, but also by measuring the PL decay times τ, which is a preferred approach as discussed below. We optimized two types of highly responsive PPD structures: (1) PPDs with wide band responsivity that are suitable for light detection over a broad spectral range, and (2) PPDs designed so that they are sensitive only over a narrow band, which makes them more specific and suitable for development of multi-analyte compact sensors arrays, with analytes that are detected in different spectral ranges. We demonstrate the functionality of such PPDs for monitoring gas-phase and dissolved oxygen (DO), as well as glucose whose monitoring is based on DO level measurements. In contrast to PPDs, the use of OPDs failed previously, with only measurements of I enabling O_2 monitoring [12,18].

The high-responsivity PPDs together with their response time of $\sim$ 500 ns (that can be further reduced [13] enabled reliable analyte sensing. Using PPDs, oxygen and glucose monitoring sensitivity was comparable or better than with a commercial Si PD.

PL-based O_2 sensors have been studied extensively [28–38], and such PL-based gas-phase and DO monitors are available commercially. Development of such sensors continues for applications such as medical, biological, and water treatment, and for developing reliable and sensitive compact field-deployable devices. The PL-based sensors are advantageous due to their high sensitivity, low maintenance, and infrequent need for calibration. Typically an oxygen-sensitive dye (*e.g.*, Pt or Pd octaethylporphyrin; PtOEP or PdOEP, respectively) is embedded in a thin polymeric (*e.g.*, polystyrene, PS) or sol-gel film. When the photoexcited dye molecules collide *via* a Dexter mechanism with

oxygen molecules, their PL is quenched with a dose-dependent decrease in I and τ. Calibration lines and the oxygen level can be obtained (ideally for a dynamic quenching process [39]) using the Stern-Volmer (S-V) equation:

$$I_0/I = \tau_0/\tau = 1 + K_{SV}[O_2], \qquad (1)$$

where I_0 and τ_0 are the unquenched values and K_{SV} is the film- and temperature-dependent S-V constant. The sensitivity S is defined as

$$S \equiv I_0/I(100 \text{ \% } O_2) = \tau_0/\tau(100 \text{ \% } O_2). \qquad (2)$$

Pulsing the excitation source enables monitoring O_2 *via* τ measurements. This approach is valid provided that τ is significantly longer than the electroluminescence (EL) decay time of the excitation source and the PD's response time. Monitoring τ is advantageous as it eliminates the problem of stray or other background light. Additionally, when operating in the τ mode, moderate changes in the sensor components, including dye leaching, have a minimal effect on the sensor's response. As a result, the need for frequent calibration and optical filters is eliminated, which can lead to more compact and reliable devices.

As mentioned, glucose monitoring is based on determining the DO level. Glucose is catalytically oxidized in the presence of glucose oxidase (GOx) and O_2 to yield gluconic acid with the oxygen reduced to H_2O_2. In sealed containers, where there is no supply of DO beyond the initial concentration, the change in [DO] is equal to the change in the initial glucose concentration [glucose]$_{initial}$ if [glucose]$_{initial} \leq$ [DO]. As the analyte conversion into products is complete, [DO]$_{final}$ is given by

$$[DO]_{final} = [DO]_{initial} - [glucose]_{initial} \qquad (3)$$

and the SV equation becomes

$$I_0/I = \tau_0/\tau = 1 + K_{SV} \times \{[DO]_{initial} - [glucose]_{initial}\} \qquad (4)$$

Thus, a plot of $1/\tau$ *vs.* [glucose]$_{initial}$, to generate calibration lines, will ideally be linear up to [glucose]$_{initial}$ = [DO]$_{initial}$.

In some sensing films, not all of the sensing molecules are in the same state, hence, a two-site model may better fit the experimental data [40]. This situation can occur if the oxygen diffusion through the (*e.g.*, polystyrene, PS) matrix is impeded. The equation describing the two-state model is given by [40]

$$I_0/I = (f_0/(1 + K_{SV}[O_{2applied}]) + (1-f_0)/(1 + K_{SV}[O_{2atmosphere}]))^{-1} \qquad (5)$$

It is assumed that K_{SV} is the same for both states, and that the O_2 concentration of the second state is equivalent to the atmospheric level due to the PS matrix trapping of the gas. f_0 denotes the fraction of the active dye molecules that are in the first state, with the rest of the active dye molecules being in the second state. We note that various models were developed over time [41]; we chose the two-state model for simplicity and as the data fitting for a PdOEP sensing film was good.

2. Methods

The sensor components used for measuring gas-phase O_2, DO, and glucose included PtOEP or PdOEP embedded in PS as sensing films, a 5 mw 385 nm LED as the excitation source, and broadband PPDs or narrowband PPDs; a commercial Si photodiode reference was also used. The PtOEP was purchased from H. W. Sands, the PdOEP from Frontier Scientific, the 280,000 MW PS from Sigma Aldrich, and the LED and Si photodiode from Thorlabs.

A low pass filter in front of the LED and a long pass filter in front of the PD were used when using the broadband measurement setup. The former was needed as the 385 nm LED has a small emission peak at $\sim$ 600 nm that interferes with the $\sim$ 630 nm sensor film peak PL. For the narrowband PPD setup, the filter between the sensing film and the PD was not required.

The PD signal, with no applied bias, was amplified 5x using a Stanford Research Systems (SRS) amplifier model SR445A and then

amplified 5,000x using a SRS low-noise preamplifier model SR560. It was recorded using a Tektronix TDS7104 Oscilloscope, and analyzed using LabVIEW. The LED was pulsed at 3.9 V for narrow band and 3.5 V for broadband PDs for 100–300 μs, depending on oxygen concentration, at a rate of 100 Hz. The NB PPDs required a higher LED voltage (higher brightness) due to their lower EQE in comparison to that of the BB PPDs. The longer 300 μs pulse was used additionally for 0 and 10 % O_2 to ensure the signal reached a steady state for intensity measurements. The experiment was automated by a homemade LabVIEW program that controlled pulse parameters, data recording, timing, and the oxygen concentration through a MKS multi-gas controller 647B with oxygen and argon mixtures. The sensing film was exposed to each oxygen concentration for 3 min to ensure equilibration; the signal was averaged over 3 min.

The broad band PPDs have a structure of indium tin oxide (ITO)/ poly[bis(4-phenyl)(2,4,6-trimethylphenyl)amine](PTAA)/perovskite ($Cs_{0.05}FA_{0.08}MA_{0.15}PbI_3$, where FA is formamidinium and MA is methylamine)/fullerene (C_{60})/bathocuproine (BCP)/Cu. The ITO substrate was treated under UV-Ozone for 20 min. The PTAA layer was next spin coated from a toluene solution containing 0.2 wt% PTAA at 4000 rpm for 35 s. Next, it was annealed at 100 °C for 10 min. The perovskite precursor solution was spin coated at 2000 rpm for 2 s and 4000 rpm for 20 s onto the PTAA layer and further annealed at 100 °C for 10 min. After that, 20 nm C_{60}, 8 nm BCP, and 80 nm Cu were sequentially deposited by thermal evaporation. For narrow band PPDs, the device with perovskite-2 active layer only was first fabricated with the same structure. The perovskite-1 filter layer was then coated onto the glass side of the standard PPD device to complete the fabrication of narrow band PPDs.

The EQE spectrum of the PPDs was measured with a Newport IPCE measurement system under zero bias and a 35 Hz modulated light.

The PtOEP was embedded in PS by dissolving both materials in toluene at a ratio of 1:40 PtOEP:PS with a PtOEP concentration of 1 mg/ mL. The solution was drop cast on a 1"x1" glass and annealed at 65 °C for 1 h to evaporate the solvent while outgassing oxygen from the film.

Both S-V ratios τ_0/τ and I_0/I were measured. As mentioned, I was measured after a steady state was reached, and τ was obtained by fitting the PL decay curves, following the LED pulse, to either a single or double exponential decay, depending on the O_2 level, using a homemade MATLAB program.

Glucose monitoring was performed using PPDs and a PtOEP:PS film submerged in a phosphate buffer solution (PBS) obtained from Fischer Scientific and containing glucose oxidase from Sigma Aldrich. The PtOEP:PS film was drop cast on the bottom of a 23.5 mL vial. The vial was sealed with a plastic film and covered with a lid to isolate the solution from atmospheric oxygen.

3. Results and discussion

3.1. Broad-band (BB) PPDs

Utilization of a BB hybrid PPD with high responsivity and fast

response time is demonstrated first for gas-phase O_2 monitoring. Fig. 1(a) and Fig. 1(b) show the PPD's structure and EQE spectrum, respectively [13,42,43]. The layer thicknesses are shown in the figure. As seen, the EQE is high (~85 %) and constant across a broad wavelength range of ~375 to ~775 nm. The response time was measured with transient photocurrent (TPC), as shown in Fig. 1(c). By fitting the photocurrent decay, the response time of the BB PPD device was determined to be 536 ns. This response time is limited by the RC constant of the large area devices, which is however fast enough for the application reported here. The PPD's response to light, *i.e.*, current density *vs* light intensity, is linear over more than ~8 orders of intensity magnitude [13].

In Testing the PPD for analyte monitoring, we used a 385 nm LED excitation source and a thin sensing film of PtOEP embedded in a PS matrix (~8 μm thick). PtOEP has absorption bands peaking at 385 nm and 535 nm, with the former being ~5x more intense; the dye emits in the red, with a peak PL at ~635 nm [1,10]. The shortest τ of O_2 sensors is obtained when the sensing film is exposed to 100 % gas-phase oxygen; it is typically ~3-5 μs depending on the matrix. As such the hybrid PPD is a viable option for monitoring O_2 *via* the advantageous τ mode (Fig. 2).

As seen, the S-V plots are linear over the whole $[O_2]$ range with similar results obtained in both I and τ modes; S exceeded 16. The ability to perform such a measurement in the τ mode is far beyond the capability of previous OPDs or inorganic thin film PDs based on a-Si:H or nc-Si.

3.2. Narrow-band (NB) PPDs

Fig. 3(a) shows a photograph of both the BB and NB PPDs in ambient light. As seen, the NB PPD, unlike the BB PPD, appears red due to a structurally integrated thin filter that allows only red light to pass through it. The device structure with the Perovskite-1 filter and the Perovskite-2 active layer is shown in Fig. 3(b).

Perovskite-1 was a ~1 μm thick (to ensure a good filtering effect) $MAPbI_{0.6}Br_{2.4}$ filter with the absorption edge at ~650 nm cast on the air-side of the glass substrate. In fact, the absorption edge of the Perovskite-1 layer is tunable. By changing the bromine to iodine ratio, it could be varied from ~550 nm to ~800 nm. The ~500 nm thick Perovskite-2 active layer was $Cs_{0.4}FA_{0.6}PbIBr_2$ with the absorption edge at ~680 nm. This thickness ensures efficient light absorption and charge collection. Fig. 4(a) shows the absorption spectra of both Perovskite-1 and Perovskite-2, whose combination filters short wavelength photons (< 600 nm), guaranteeing the narrow band response range of 610 nm – 680 nm. Fig. 4 shows also the attributes of an ~8 mm^2 NB PPD, *i.e.*, the EQE spectrum and the response curve.

As seen, the absorption band of the PPD is narrow, peaking at ~645 nm, successfully designed for the ~635 nm PtOEP PL peak; shorter wavelengths are filtered out. This filtering approach is easy to implement and it adds only an integrated solution-processed ~1 μm tunable film. The response time of this NB PPD was ~540 ns, significantly faster than the PL decay times of the sensing film. The
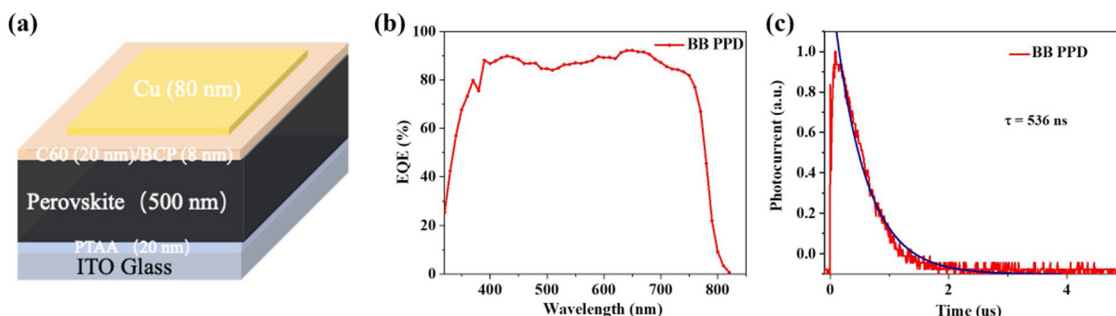

Fig. 1. (a) the structure of the broad band (BB) PPD, (b) EQE spectrum, and (c) the response time of the BB PPD.
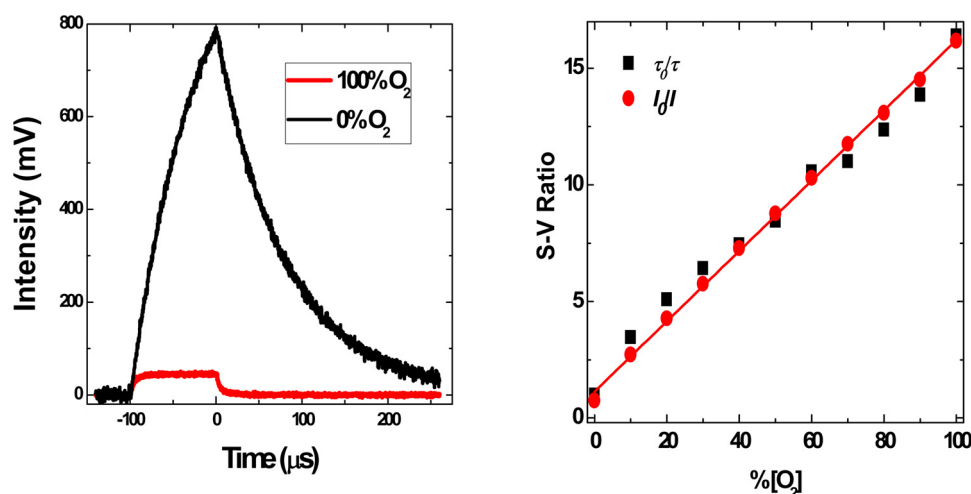
Fig. 2. (a) The PL intensity *vs* time at 0 and 100 % gas-phase oxygen. (b) The S-V plots for *I* and τ modes. A LED with peak emission at 385 nm and a broad band PPD were used.

performance of these NB PPDs exceeds that of OPDs that were previously used in all-organic sensors [12,18], in particular when measuring τ, which was impossible with those previous OPDs. It also equals or exceeds that of commercial Si PDs, as demonstrated in Fig. 5. The figure shows the gas-phase S-V line using both the NB PPD and a commercial Si PD, with the former showing $S \sim 20$. The excitation and decay curves for DO are also shown; the LED pulse duration was 400 μs with τ shortening as the DO level increases. Importantly, with the NB PPD the filter in front of the PD is unnecessary, which can result in more compact sensors for multiple analytes.

3.3. Glucose monitoring

As mentioned, in the presence of glucose oxidase and oxygen, glucose is oxidized consuming DO in a stoichiometric reaction. As the glucose level increases, DO is increasingly consumed, and when the reaction is performed in a closed cell to prevent replenishment of oxygen from the gas phase, Eq. 4 is ideally obeyed. Fig. 6 shows an example of a glucose sensor operated in the τ mode using the NB PPD. As seen, Eq. 4 is obeyed up to ~ 0.26 mM glucose, which is the DO level at room temperature in equilibrium with air. Beyond ~ 0.26 mM glucose (*i.e.*, when the DO is completely consumed) τ remains constant as shown in Fig. 6.

We previously demonstrated simultaneous monitoring of glucose, lactate, and ethanol (all of which are oxidized in similar reactions as that of glucose with their specific oxidase enzymes) in mixtures [10,30], thus this setup could be used for any of these analytes. The analytes were previously monitored by measuring changes in *I*, with the τ mode measurement possible only with commercial Si PDs. As mentioned, monitoring analytes in the τ mode, which is possible with the

PPDs, is advantageous as it eliminates the need for optical filters and frequent calibration, because it is independent of small changes in the intensity of the light source and stray light.

3.4. Sensing film: PdOEP vs PtOEP

In addition to PtOEP:PS, PdOEP:PS films were also tested to demonstrate their compatibility with PPDs. Fig. 7 shows the S-V [O_2] monitoring results using a NB PPD. The S-V data can be fit linearly up to 30 % O_2, but above 30 % the fit requires assuming more than one O_2 state. The line presenting the data in Fig. 7 uses a two-site equation, where one site is in equilibrium with the gas-phase O_2 level, while the other site is at atmospheric O_2 concentration. As seen, this "Two-Site Model" successfully describes the PdOEP S-V line [40]. The fit shows that ~ 19 % of PdOEP sites are exposed to atmospheric O_2 trapped in the PS matrix. From Fig. 7 it is clear, as expected, that PdOEP is more suitable than PtOEP for detecting low O_2 levels. This is due to PdOEP's larger sensitivity associated with the longer τ (~ 1 ms) at 0 % O_2 in comparison to that of PtOEP, which is ~ 100 μs.

4. Summary and concluding remarks

The promising utilization of fast and tunable BB and NB PPDs for sensitive and reliable optical detection of (bio)analytes, including in the preferred τ mode, is shown for the first time. With their further integration with OLED excitation sources, compact devices can be achieved for monitoring a variety of analytes, including simultaneous detection of multi-analytes. Using BB PPDs in conjunction with microcavity OLEDs that have narrow EL bands peaking at tunable wavelengths from blue to green, a highly responsive spectrometer on a chip
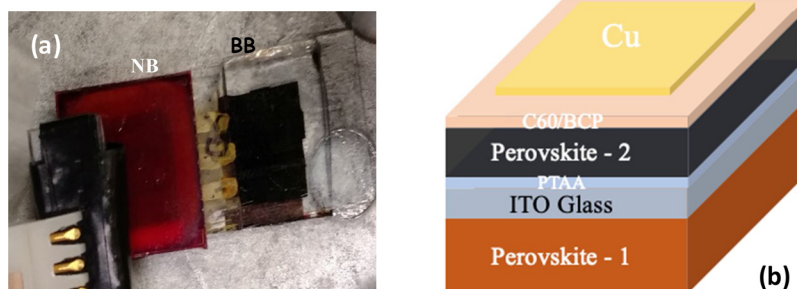

Fig. 3. (a) a photograph of the BB and NB (red) PPDs and (b) the structure of the NB PPD. The red color of the NB PPD is due to the Perovskite-1 filter (For interpretation of the references to colour in this figure legend, the reader is referred to the web version of this article).
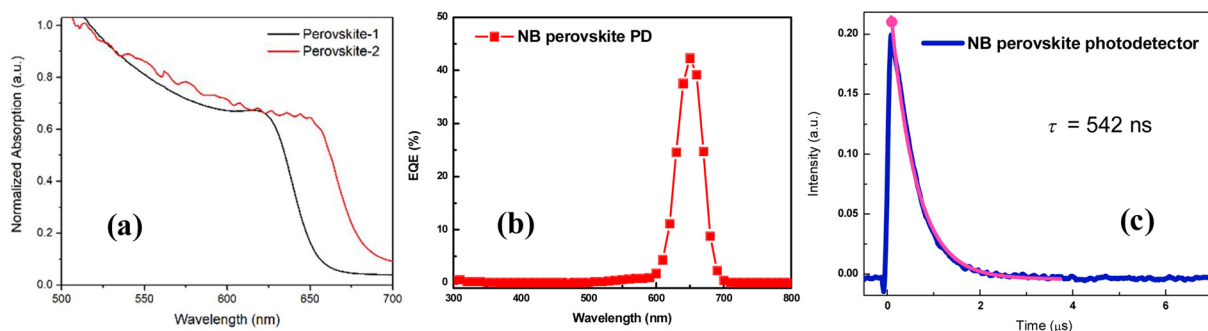
Fig. 4. (a) Absorption spectra of the Perovskite-1 and Perovskite-2 layers, (b) The EQE spectrum of the NB PPD, and (c) The NB PPD response curve.
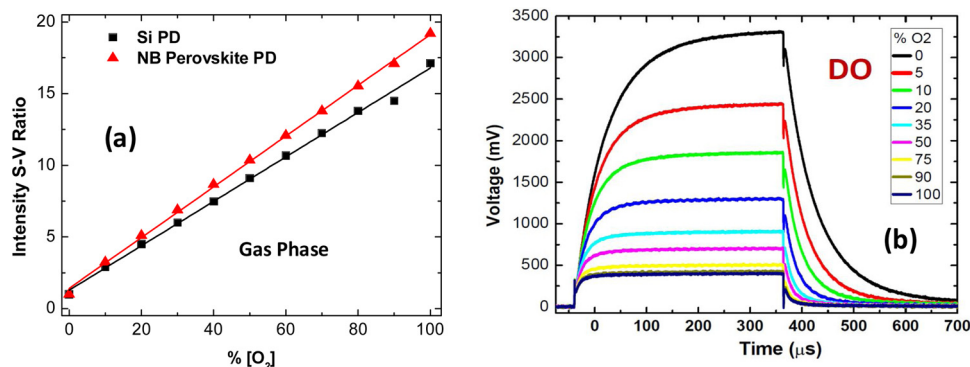

Fig. 5. (a) The S-V lines of gas-phase O_2 sensing obtained with NB PPD and a Si photodiode and (b) excitation and decay curves of a NB PPD used for DO monitoring; the numbers indicate the gas phase level that is in equilibrium with the solution.
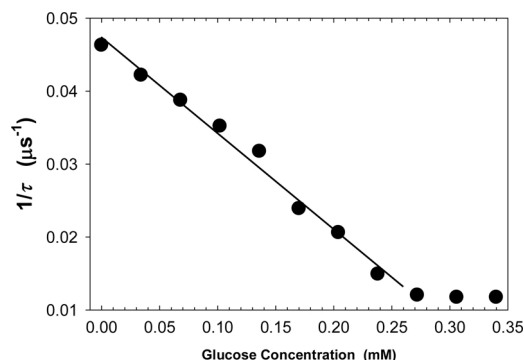

Fig. 6. Monitoring glucose using a 385 nm pulsed LED and a NB PPD with peak absorption at ~645 nm.

can be achieved, as was previously shown with OPDs. With the NB PPDs, an array for monitoring multiple analytes with different, specific wavelength sensing probe emissions can similarly be realized. These PPDs show promise also for future wearable sensors.

Fig. 7. The S-V ratio of PdOEP:PS in comparison to that of PtOEP:PS from 0-100 % O_2 using NB PPDs. The line is a fit to the Two-Site Model where one site is exposed to the plotted O_2 concentration while the other site contains trapped atmospheric O_2.

Credit author statement

JW conducted the sensing experiments at Iowa State University (ISU) and participated in writing the paper.

MF performed sensing experiments at ISU and assisted with the experimental setup at ISU.

ED and RK assisted with the experiments at ISU.

XX and NJL fabricated the PPDs at the University of North Carolina (UNC) and characterized them prior to shipment to ISU.

RS wrote the paper, with contributions from JS and JH.

RS, JS, and JH conceived the project, obtained the NSF funding, and mentored the graduate students who participated in the project.
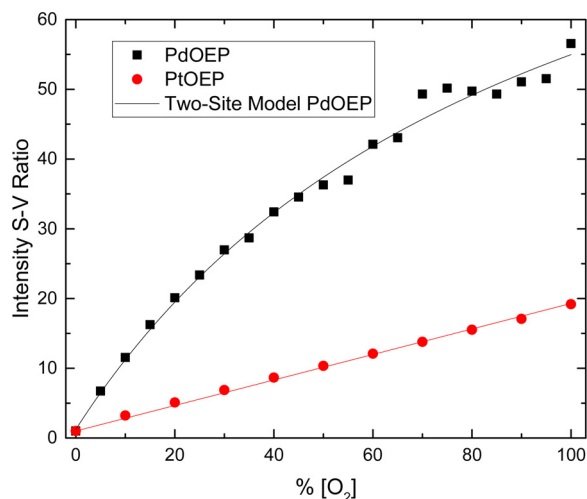
Declaration of Competing Interest

The authors declare that they have no known competing financial interests or personal relationships that could have appeared to influence the work reported in this paper.

Acknowledgements

References

[1] R. Shinar, J. Wolanyk, R. Kaudal, J.M. Park, J. Shinar, Organic and hybrid electronics in optical analytical applications, Mater. Matters 14 (2019) 19.

[2] M. Prosa, M. Bolognesi, L. Fornasari, G. Grasso, L. Lopez-Sanchez, F. Marabelli, S. Toffanin, Nanostructured organic/hybrid materials and components in miniaturized optical and chemical sensors, Nanomater. 10 (2020) 480.

[3] Y. Xia, L.E. Aguirre, X. Xu, O. Inganäs, All-polymer high-performance photodetector through lamination, Adv. Elec. Mater. 6 (2020) 7 1901017.

[4] A. Smith, Y. Cai, S. Vengasandra, R. Shinar, J. Shinar, Advances toward commercialization of a new generation of low cost (O)LED-based dissolved oxygen and bioanalyte monitors, organic semiconductors in sensors and bioelectronics III, in: R. Shinar, I. Kymissis (Eds.), SPIE, Bellingham, WA, SPIE Conf. Proc. 7779 (2010) 77790P-1–77790P-10.

[5] L. Meng, Y. Zhang, X. Wan, C. Li, X. Zhang, Y. Wang, X. Ke, Z. Xiao, L. Ding, R. Xia, H.-L. Yip, Y. Cao, Y. Chen, Organic and solution-processed tandem solar cells with 17.3% efficiency, Science 361 (2018) 1094–1098.

[6] H.-H. Gao, Y. Sun, X. Wan, X. Ke, H. Feng, B. Kan, Y. Wang, Y. Zhang, C. Li, Y. Chen, A new nonfullerene acceptor with near infrared absorption for high performance ternary-blend organic solar cells with efficiency over 13%, Adv. Sci. 5 (2018) 6 1800307.

[7] F. Yang, W. Zhao, Q. Zhu, C. Li, W. Ma, J. Hou, W. Li, Boosting the performance of non-fullerene organic solar cells via cross-linked donor polymers design, Macromol. 52 (2019) 2214–2221.

[8] A.K. Bansal, S. Hou, O. Kulyk, E.M. Bowman, I.D.W. Samuel, Wearable organic optoelectronic sensors for medicine, Adv. Mater. 27 (2015) 7638–7644.

[9] D. Han, Y. Khan, J. Ting, S.M. King, N. Yaacobi-Gross, M.J. Humphries, C.J. Newsome, A.C. Arias, Flexible blade-coated multicolor polymer light-emitting diodes for optoelectronic sensors, Adv. Mater. 29 (2017) 8 1606206.

[10] J. Shinar, R. Shinar, Organic light-emitting devices (OLEDs) and OLED-based chemical and biological sensors: an overview, J. Phys. D Appl. Phys. (2008), p. 26 133001.

[12] E. Manna, F. Fungura, R. Biswas, J. Shinar, R. Shinar, Tunable near UV microcavity OLED arrays: characterization and analytical applications, Adv. Funct. Mater. 25 (2015) 1226–1232.

[13] L. Li, Y. Deng, C. Bao, Y. Fang, H. Wei, S. Tang, F. Zhang, J. Huang, Self-filtered narrowband perovskite photodetectors with ultrafast and tuned spectral response, Adv. Opt. Mater. 5 (2017) 6 1700672.

[14] X. Xiao, C. Bao, Y. Fang, J. Dai, B.R. Ecker, C. Wang, Y. Lin, S. Tang, Y. Liu, Y. Deng, X. Zheng, Y. Gao, X.C. Zeng, J. Huang, Argon plasma treatment to tune perovskite surface composition for high efficiency solar cells and fast photodetectors, Adv. Mater. 30 (2018) 7 1705176.

[15] R.A. Street, Hydrogenated Amorphous Silicon, Cambridge University Press, Cambridge, UK, 1991.

[16] G. Yue, L. Sivec, J.M. Owens, B. Yan, J. Yang, S. Guha, Optimization of back reflector for high efficiency hydrogenated nanocrystalline silicon solar cells, Appl. Phys. Lett. 95 (2009) 3 263501.

[17] K. Nalwa, Y. Cai, A. Thoemin, R. Shinar, J. Shinar, S. Chaudhary, Polymer-based photodetectors for structurally integrated photoluminescence based oxygen sensors, organic semiconductors in sensors and bioelectronics II, Proc. SPIE 7418 (2009) 74180F-1–74180F-7.

[18] E. Manna, T. Xiao, J. Shinar, R. Shinar, Organic photodetectors in analytical applications, Electronics 4 (2015) 688–722.

[19] W. Wang, D. Zhao, F. Zhang, L. Li, M. Du, C. Wang, Y. Yu, Q. Huang, M. Zhang, L. Li, J. Miao, Z. Lou, G. Shen, Y. Fang, Y. Yan, Highly sensitive low-bandgap perovskite photodetectors with response from ultraviolet to the near-infrared region, Adv. Funct. Mater. 27 (2017) 7 1703953.

[20] Z. Zhao, J. Wang, C. Xu, K. Yang, F. Zhao, K. Wang, X. Zhang, F. Zhang, Photomultiplication type broad response organic photodetectors with one absorber layer and one multiplication layer, J. Phys. Chem. Lett. 11 (2020) 366–373.

[21] Y. Fang, Q. Dong, Y. Shao, Y. Yuan, J. Huang, Highly narrowband perovskite single-crystal photodetectors enabled by surface-charge recombination, Nat. Phot. 9 (2015) 679–686.

[22] L. Shen, Y. Fang, D. Wang, Y. Bai, Y. Deng, M. Wang, Y. Lu, J. Huang, A self-powered, sub-nanosecond-response solution-processed hybrid perovskite photodetector for time-resolved photoluminescence-lifetime detection, Adv. Mater. 28 (2016) 10794–10800.

[23] M. Ahmadi, T. Wu, B. Hu, A review on organic–inorganic halide perovskite photodetectors: device engineering and fundamental physics, Adv. Mater. 29 (2017) 24 1605242.

[24] Q. Lin, A. Armin, P.L. Burn, P. Meredith, Filterless narrowband visible photodetectors, Nat. Phot. 9 (2015) 687–694.

[25] A. Armin, R. Jansen-van Vuuren, N. Kopidakis, P. Burn, P. Meredith, Narrowband light detection via internal quantum efficiency manipulation of organic photodiodes, Nat. Commun. 6 (2015) 8 6343.

[26] W. Wang, F. Zhang, M. Du, L. Li, M. Zhang, K. Wang, Y. Wang, B. Hu, Y. Fang, J. Huang, Highly narrowband photomultiplication type organic photodetectors, Nano Lett. 17 (2017) 1995–2002.

[27] W. Wang, M. Du, M. Zhang, J. Miao, Y. Fang, F. Zhang, Organic photodetectors with gain and broadband/narrowband response under top/bottom illumination

[28] R. Liu, T. Xiao, W. Cui, J. Shinar, R. Shinar, Multiple approaches for enhancing all-organic electronics photoluminescent sensors: simultaneous oxygen and pH monitoring, Anal. Chim. Acta 778 (2013) 70–78.

[29] R. Liu, Z. Ye, J.M. Park, M. Cai, Y. Chen, K.-M. Ho, R. Shinar, J. Shinar, Microporous phase-separated films of polymer blends for enhanced outcoupling of light from OLEDs, Opt. Exp. 19 (S6) (2011) A1272–A1280.

[30] Y. Cai, R. Shinar, Z. Zhou, C. Qian, J. Shinar, Multianalyte sensor array based on an organic light emitting diode platform, Sens. Actuators B Chem. 134 (2008) 727–735.

[31] S. Vengasandra, Y. Cai, D. Grewell, J. Shinar, R. Shinar, Polypropylene CD-organic light-emitting diode biosensing platform, Lab Chip 10 (2010) 1051–1056.

[32] D.C. Duffy, H.L. Gillis, J. Lin, N.F. Sheppard, G.J. Kellog, Microfabricated centrifugal microfluidic systems: characterization and multiple enzymatic assays, Anal. Chem. 71 (1999) 4669–4678.

[33] J. Zhang, Q. Guo, M. Liu, J. Yang, A lab-on-CD prototype for high-speed blood separation, J. Micromech. Microeng. 18 (2008) 6 125025.

[34] A.S. Watts, A.A. Urbas, E. Moschou, V.G. Gavalas, J.V. Zoval, M. Madou, L.G. Bachas, Centrifugal microfluidics with integrated sensing microdome optodes for multiion detection, Anal. Chem. 79 (2007) 8046–8054.

[35] D.D. Nolte, Review of centrifugal microfluidic and bio-optical disks, Rev. Sci. Instrum. 80 (2009) 22 101101.

[36] D. Ghosh, R. Shinar, V. Dalal, Z. Zhou, J. Shinar, Amorphous and nanocrystalline p–i–n Si and Si,Ge photodetectors for structurally integrated O_2 sensors, J. Non-Crystalline Sol. 354 (2008) 2606–2609.

[37] K.S. Nalwa, Y. Cai, A.L. Thoeming, J. Shinar, R. Shinar, S. Chaudhary, Polythiophene-fullerene based photodetectors: tuning of spectral response and application in photoluminescence based (bio)chemical sensors, Adv. Mater. 22 (2010) 4157–4161.

[38] Z. Zhou, R. Shinar, A.J. Allison, J. Shinar, Enhanced photoluminescence of oxygen sensing films through doping with high dielectric constant particles, Adv. Func. Mat. 17 (2007) 3530–3537.

[39] E.R. Carraway, J.N. Demas, B.A. DeGraff, J.R. Bacon, Photophysics and photochemistry of oxygen sensors based on luminescent transition-metal complexes, Anal. Chem. 63 (1991) 337–342.

[40] J.N. Demas, B.A. DeGraff, W. Xu, Modeling of luminescence quenching-based sensors: comparison of multisite and nonlinear gas solubility models, Anal. Chem. 67 (1995) 1377–1380.

[41] Y. Cai, A. Smith, J. Shinar, R. Shinar, Data analysis and aging in phosphorescent oxygen-based sensors, Sens. Act. B. Chem. 146 (2010) 14–22.

[42] Y. Fang, J. Huang, Resolving weak light of sub-picowatt per square centimeter by hybrid perovskite photodetectors enabled by noise reduction, Adv. Mater. 27 (2015) 2804–2810.

[43] X. Xiao, J. Huang, unpublished results.

Joshua Peter Wolanyk recived a BA in physics from Gustavus Adolphus College. He is currently pursuing a MSc in electrical engineering and a Ph.D. in condensed matter physics at Iowa State University. His PhD focuses on using organic semiconductors in sensing setups and looking at degradation of organic photovoltaics.

Xun Xiao is a PhD graduate student at the University of North Carolina (UNC) in Chapel Hill. His interests include perovskite solar cell materials and devices.

Michael Fralaide is a PhD student in Electrical and Computer Engineering at Iowa State University. His interest include light extraction from OLED and all organic/hybrid optical chemical and biological sensors.

Nicholas J. Lauersdorf received his BS in Physics and Mathematics from the University of Wisconsin-Madison in 2018. He is currently a graduate student at the University of North Carolina at Chapel Hill. His research interests mainly focus on improving the measurement capabilities of perovskite photodetectors.

Rajiv Kaudal received an MSc in Electrical and Computer Engineering from Iowa State University (ISU). He completed his PhD in Physics and Astronomy at ISU in April 2020. His research focuses on basic and applied topics in organic electronics, in particular light extraction from OLEDs and OLED applications in chemical and biological sensors.

Erik Dykstra is a PhD student in Physics & Astronomy at Iowa State University. His interest include light extraction from OLEDs and all organic/hybrid optical chemical and biological sensors.

Jinsong Huang received his PhD in Materials Science and Engineering from UCLA in 2007. He is currently a Professor of Applied Physical Sciences at the University of North Carolina (UNC) in Chapel Hill. Prior to UNC he was the Susan Rosowski University Professor in the Department of Mechanical and Materials Engineering, University of Nebraska, Lincoln. His current research is on perovskite solar cells and involves device engineering, material processing, and chemistry for record energy conversion efficiency and stability.

Joseph Shinar received his PhD in Physics from the Hebrew University, Jerusalem, Israel. He is currently a Senior Physicist at the Ames Laboratory – USDOE, Professor of Physics and Astronomy, and Courtesy Professor of Electrical and Computer Engineering at Iowa State University (ISU). He joined ISU in 1985 following a postdoctoral position in

the Physics Department of the University of California, Santa Barbara. His research interests include organic semiconductor materials and device physics, OLEDs, OLED-based chemical and biological sensors, and organic & hybrid photovoltaics.

Ruth Shinar is a Senior Scientist at the Microelectronics Research Center and an Adjunct Professor of Electrical and Computer Engineering at Iowa State University (ISU). She received her PhD in Physical Chemistry in from the Hebrew University, Jerusalem, Israel. She joined ISU in 1985 following a postdoctoral position in the Chemistry Department of the University of California, Santa Barbara. Her research interests include OLEDs, organic and hybrid photovoltaics, and all-organic/hybrid chemical and biological sensors.